Heat and Mass Transfer Research Journal
Vol. 3, No. 2; 2019
Published by CanSRG
http://cansrg.com/journals/hmtrj/

Evaluation of Crossflow Heat Exchanger Modules in Sequential and Simultaneous Orientations

Mohammed Ismail[1,*], Mesbah G. Khan[2] and Amir Fartaj[1]

[1] *Department of Mechanical Automotive and Materials Engineering, University of Windsor, Windsor, Canada.*
[2]*Sanden International (U.S.A.) Inc., Plymouth, MI, U.S.A.*

Abstract

Heat exchangers are the key components in automotive, residential and industrial heat transfer applications. These are employed in thermal management systems, as well as heating, ventilation, air conditioning and refrigeration systems. In this research, two distinct heat exchanger modules, sequential and simultaneous, are modeled to evaluate their heat transfer. The simultaneous heat exchanger module is used as the replacement candidate of the conventional sequential module to further enhance convective heat transfer. The study uses three-dimensional domains to resolve flow and heat transfer in air-to-liquid crossflow orientation. A finite volume method based ANSYS FLUENT computational fluid dynamics (CFD) code is used to conduct the numerical simulations. First, fundamental laminar heat transfer and flow parameters are investigated in both modules of flat tube heat exchanger (FTHX). Next, the minichannel heat exchanger (MICHX) is employed in replacement of the conventional FTHX. Water with temperatures of 65℃ (MT-HX) and 95℃ (HT-HX) for the core Reynolds number range of 350≤Re≤2250 is cooled by crossflow cold air temperature of 25℃ and velocity of 6m/s. For an identical module size, the simultaneous module heat transfer outperforms the benchmark sequential module. The MICHX module provides even more heat transfer over the FTHX module.

Keywords: *crossflow; heat transfer; sequential and simultaneous modules; laminar flow; flat tube; minichannel.*

Nomenclature

3D	Three-dimensional
A	Area [m^2]
Al	Aluminum
A_s	Heat transfer surface area [m^2]
c_p	Fluid specific heat [J/kgK]
d	Channel diameter [m]
D_h	Hydraulic diameter [m]
Expt	Experimental
h	Heat transfer coefficient [w/m^2K]
HVAC	Heating, ventilation and air conditioning
HT	High temperature (95℃)
HX	Heat exchanger
k	Thermal conductivity [w/mK] Turbulence kinetic energy [m^2/s^2], or [J/kg]
L	Channel length [m]
m	Mass [kg]
$\dot{m}$	Mass flow rate [kg/s]
MICHX	Minichannel heat exchanger
MMT CO_2	Million metric tonnes of carbon dioxide
MT	Medium temperature (65℃)
Mtoe	Million tonnes of oil equivalent
Nu	Nusselt number
num	Numerical
Pr	Prandtl number
$\dot{Q}$	Heat transfer rate [w]
Re	Reynolds number
T	Temperature [℃]
T_i	Fluid inlet temperature [℃]
T_o	Fluid outlet temperature [℃]
T_m	Mass weighted average temperature of fluid [℃]
T_s	Channel inner surface temperature [℃]
V	Fluid mean velocity [m/s]

Greek letters

ρ	Density [kg/m^3]

* Corresponding Author
Submitted: September 21, 2019 Revised: December 12, 2019 Accepted: December 13, 2019

μ	Fluid dynamic viscosity [kg/ m. s or N. s/m^2]	Δ	Change in variable
		Δp	Pressure drop [kPa]
ν	Momentum diffusivity [m^2/s]	ΔT	Temperature difference [°C]
ε	Turbulence kinetic energy dissipation rate [m^2/s^3]		

Subscripts

a	Air	m	Mean, mass weighted average
c	Cross-sectional	michx	Minichannel heat exchanger
ch	Channel	mt	Medium temperature (65℃)
enh	Enhancement	num	Numerical
expt	Experimental	o	Outlet
fr	Frontal	s	Channel inner surface
fthx	Flat tube heat exchanger	ser	Serpentine
ht	High temperature (95℃)	seq	Sequential
hy	Hydrodynamic	sim	Simultaneous
i	Inlet	th	Thermal
l	Liquid	w	Water, wall

1. Introduction

Heat is one of the most significant forms of energy that has versatile applications in our daily life. Industries cannot be imagined without the use of heat energy. The Global Energy Statistical Yearbook 2018 reported, in 2017, the global total primary energy consumption was 14,126 million tonnes of oil equivalent (Mtoe), which is increased by 2.3% compared to that of 2016 [1]. This consumed energy comes from different sources, for example, fossil, nuclear, renewable, and chemical reactions etc. Fossil fuels are explicitly connected to global warming and environmental degradation [2]. In 2017, fossil fuel was worldwide the single source for 85.2% of the energy produced as reported by BP Statistical Review of World Energy 2018 [3].

Even though natural renewable energy sources, such as sunlight, wind, tidal waves, geothermal etc. are widely available, the reserves of non-renewable energy, for example, fossil fuel and other mineral energy resources are being reduced every day. The reserves of energy sources have been gradually diminishing because of their continuous use in domestic, commercial, transportation and industrial sectors on a daily basis. In any case, energy sources are limited, which need to be conserved. Appropriate use of energy is the key to sustainable cost-effective as well as socio-economic development [2]. The U.S. Greenhouse Gas Inventory Report: 1990-2015 [2] reported that in 2015, U.S. greenhouse gas emissions totaled 6,586.7 million metric tonnes of carbon dioxide (MMT CO_2) equivalents. It also reported that U.S. emissions decreased by 2.3% from 2014 to 2015.

Environment and Climate Change Canada [4] reported, in 2015, the latest yearly dataset in this report, Canada's Greenhouse Gas (GHG) emissions were 722 MMT CO_2 equivalent, which was 727 MMT in 2014. The report also stated that total emissions decreased by 16 MMT or 2.2% during the period 2005-2015. Carbon dioxide (CO_2), 79% of total emissions, is the highest contributor to Canada's GHG emissions, which mostly results from the combustion of fossil fuel. CH_4 emissions in 2015 amounted to 14% of Canada's total [4].

According to the International Organization of Motor Vehicle Manufacturers' OICA statistics [5], the total world motor vehicle production and sales in the 2016 manufacturing year were 95 million and 93.9 million, respectively. These vehicles use a huge amount of fossil fuel to produce their operating power. Performance of motor vehicle is generally evaluated in terms of fuel consumption and emissions. The strict emission regulations set by the Environmental Protection Agency (EPA) and the California Air Resources Board (CARB) can be fulfilled by

increasing the efficiency of the power train as well as the performance of heat exchangers in HVAC and engine cooling systems.

A cooling system is necessary for any automotive engine. If no cooling system is provided, parts would melt and pistons would expand due to excessive heat of the burning fuel, and cylinder head or block would get cracked while it gets cooled. On the other hand, it is undesired to run the engine at a very low temperature that may create poor oil flow, sludge formation in the oil, and poor fuel vaporization. In order to make the engine most efficient with the least amount of pollution, it is preferred to run the engine as warm as possible without overheating. For the proper functioning of the engines, vehicles need appropriate thermal management systems. Proper devices permit easy and quick heat transfer.

In the automotive industry, heat exchangers are employed in engine cooling systems as a radiator, charge air cooler, and transmission oil cooler to remove excessive heat from the transmission systems. Heat exchangers are also used in automotive air conditioning systems as a condenser, evaporator, and heater core to keep the passenger compartment comfortable. The thermal performance of heat exchangers plays a vital role on the vehicle thermal management systems, which mainly depends on working fluid, geometry, flow channel size, engine speed, flow arrangement, etc.

Researchers [6]-[22] have paid great attention from the past decades for miniaturized and energy efficient environmentally friendly narrow-channel heat exchangers that provide elevated heat transfer for a given heat duty. The investigation of heat transfer augmentation in heat exchanger started in early 1920s, and it continues to present day [11]. Numerous researchers [23]-[28] have offered reviews of the state-of-the-art techniques for intensifying heat transfer in past years. Bergles et al. [23, 24] complied several thousands of research papers on convective heat transfer from the open literature. They offered the fourth generation of heat transfer intensification. Balaras [23] reviewed intensification techniques for heat transfer surfaces in single-phase heat transport devices. These are categorized in several kinds, such as fluid, surface, compound and combined mechanisms. Tao et al. [29] proposed three possible techniques for the single-phase heat transfer augmentation. These include reducing the thermal boundary layer, growing flow interruptions, and growing the velocity gradient adjacent to the heated surface.

Kandlikar [30] presented the commonly used channel classification for a guideline of a flow passage related to the size in term of hydraulic diameter. For fully developed laminar flow in a circular channel subjected to constant surface temperature or heat flux, heat transfer coefficient of a fluid is inversely proportional to the hydraulic diameter of the flow passage [31]-[33].

It is necessary to carefully evaluate the pressure drop penalty along with the heat transfer intensifications for selecting the channel size. In order to limit the overall pressure drop, MICHXs have to be properly designed to deliver short flow lengths [34]. The flat slab of the multi-port minichannels can reduce the airside pressure drop resulting lesser blower power [13]. For a certain heat duty, the elevated heat transfer of minichannels results in shorter channel lengths. Nowadays, miniature heat exchangers are effectively and efficiently employed in many applications, and elevated pressure gradients in MICHXs basically turn into a design control in accomplishment of an appropriate heat exchanger design.

The necessity of size and weight reduction and thermal improvement of each component as well as overall system drives the advancement of compact heat exchangers [13], [14], [17]. Minichannels offer a sustainable solution to address these concerns and are likely to be commonly used in residential, commercial, and industrial applications [14].

Kim and Bullard [35] evaluated the performance of MICHX and finned round-tube condenser as a benchmark. They reported 35% reduction of refrigerant charge in the MICHX design and 35-55% reduction of core volume and weight for the identical energy efficiency ratio (EER). The performance of a unitary split system using MICHX with a conventional fin-tube outdoor coils for air conditioning and heat pumping applications were compared by Kim and Groll [36]. Authors reported that MICHX needed 23% less face area and 32% less refrigerant-side volume than that of the conventional baseline heat exchanger. The improvement in EER ranged from 1 to 6%, depending on the air-side fin density and heat exchanger orientation.

In automotive applications, the condenser is generally placed in front of the radiator in a sequential arrangement. In this pattern, condenser releases heat to the approaching ambient air, and the air gets warmer before entering the radiator. As a result, performance of the radiator, which also releases heat from the engine coolant to the ambient air, goes down compared to the situation when the radiator faces fresh ambient ram air. The performance of the radiator can be improved by modifying the arrangement of the heat exchangers module.

In this study, the radiator and condenser are proposed to place in a simultaneous arrangement, where both heat exchangers will face similar incoming or ram air with the equivalent ambient conditions. In current study, minichannel heat exchanger (MICHX) is employed as replacement of conventional flat tube heat exchanger (FTHX) for further enhancement of convective heat transfer. The proposed simultaneous MICHX module can significantly reduce the operational energy requirements in automotive applications. It can also improve life cycle climate performance (LCCP) and mitigate the stringent emission regulations set by the EPA and the CARB.

2. Numerical Methodology

Details of the CFD models including, physical device, geometry, assumptions and governing equations, grid independency, computational set up and solution procedures are presented in this section. Simulations of the three dimensional (3D) fluid flow and heat transfer have been conducted through various models of air-to-liquid crossflow conventional flat tube and minichannel heat exchangers in the current study.

2.1. Modelling the Geometry

In the current research, several models are used in numerical simulations with the purpose of evaluating the behaviour and improving thermal performance of heat exchangers. The geometric data and specifications of the models used in current research work are illustrated in Table 1.

First, a 3D model of 2-pass finned crossflow MICHX is constructed. Focusing on the flow and heat transfer fundamentals, the model is an equivalent representation of the actual MICHX device shown in Figures 1(a) and 1(b). At this stage, another model of conventional flat tube heat exchanger (FTHX) having similar flow physics is also deployed. Two distinct modules of heat exchangers, sequential module and simultaneous module have been developed using these 2-pass heat exchangers.

The sequential heat exchangers module, as illustrated in Figure 2(a), consists of two 2-pass 2-loop heat exchangers in series. In this placement, both heat exchangers face same mass flow rate of incoming ambient air, whereas the temperature of the air is different for each heat exchanger. The front heat exchanger gets the ambient air, while the rear heat exchanger receives the exit air of the front heat exchanger.

Table 1. Summary of the specifications of the model (units are in mm).

Parameters	2-pass Single loop MICHX	Sequential FTHX	Simultaneous FTHX	Simultaneous MICHX
# of channels/tube	68	1	1	68
Channel diameter/tube height	1	1	1	1
Port-to-port distance	1.463	-	-	1.463
Gap between HXs	-	24	-	-
Slab width in x-direction	100	38 x 2	100	100
Slab thickness in y-direction	2	2	2	2
Slab length in z-direction	305	305	305	305
Module height	48	92	92	92
No. of loops/flow circuits	1	4	2	2
No. of slabs in each loop	2	2	2	2
Fin density per 25.4mm	12	12	12	12
Fin height	16	16	16	16
Fin thickness	0.1	0.1	0.1	0.1
Inlet & exit tube diameter	4.76	4.76	4.76	4.76

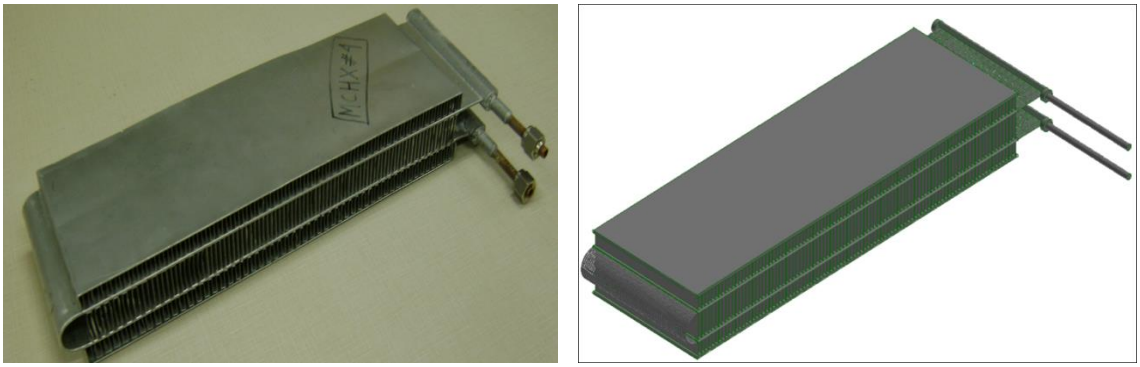

(a) (b)

Figure 1. (a) Photograph and (b) geometry of 2-pass single-loop crossflow MICHX.

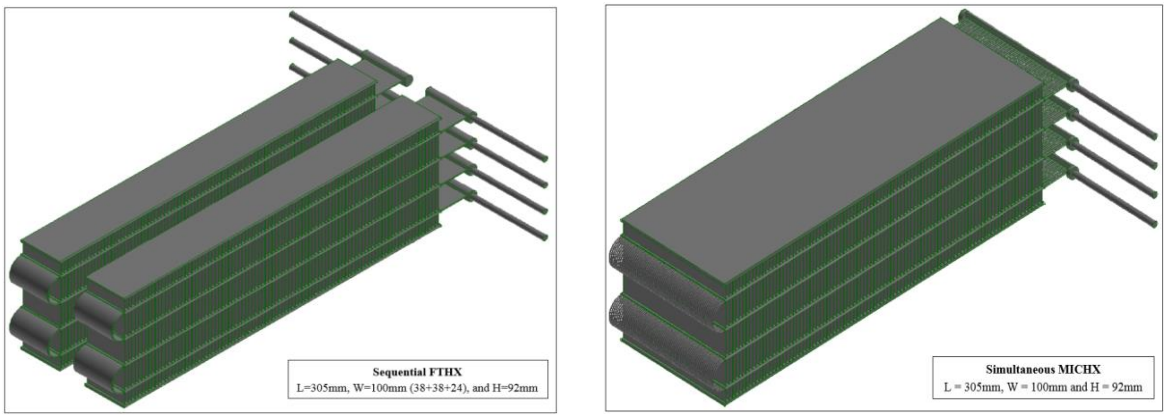

(a) (b)

Figure 2. Models of the crossflow heat exchanger module in (a) sequential and (b)simultaneous orientation.

The simultaneous heat exchangers module also uses two liquids with different operating conditions in numerical simulation. The simultaneous modules of crossflow MICHX is illustrated in Figure 3(b). Each module consists of two 2-pass single-loop heat exchangers horizontally parallel to each other. Both heat exchangers get incoming air of identical ambient conditions, such as temperature, velocity, and quality.

2.2. Computational Domains

The computational domains have been selected in consideration of the test chambers equipped in the experimental setup of the Vehicle Thermal Management Research Laboratory at University of Windsor. Each domain includes two continuums, the liquid and the air along with the solid heat exchanger. These computational domains of sequential and simultaneous modules are shown in Figure 3 and Figure 3, respectively.

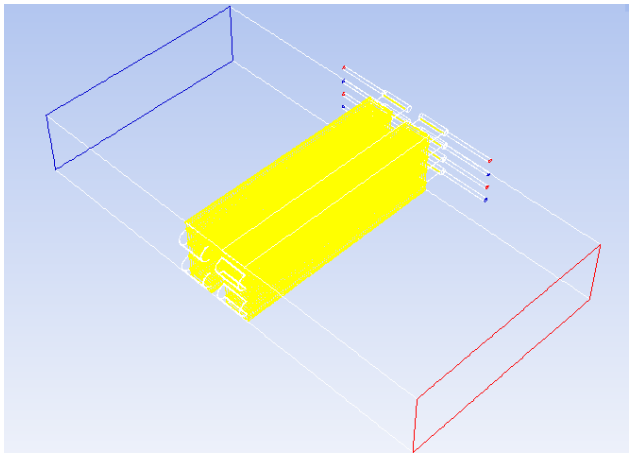

Figure 3. Computational domain of the crossflow MICHXs in sequential module.

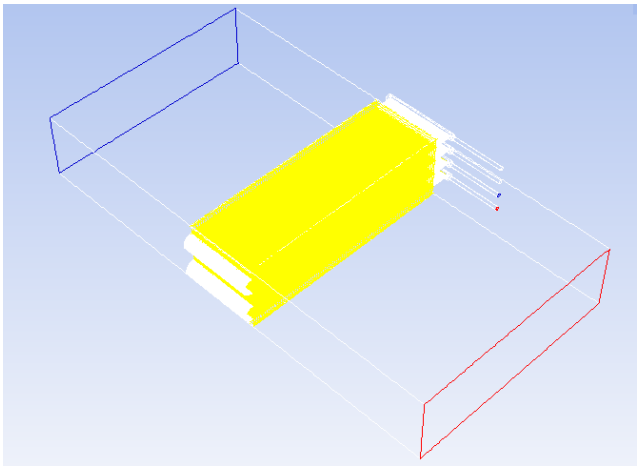

Figure 4. Computational domain of the crossflow MICHXs in simultaneous module.

2.3. Mesh Generation

Various meshing approaches have been applied to generate appropriate grids for each geometry in the computational domain. GAMBIT is used to create geometry and generate mesh applicable for CFD simulations using ANSYS FLUENT code. Every geometry contains a huge number of surfaces and volumes because of the complex shape of the models. Due to the complexity of the geometry, the model is divided into several sub-sections including air (test

chamber), manifolds, headers, serpentines, channels, and solid slabs and fins. A computer with 16 parallel processors and 128GB random access memory (RAM) is used for this current study. Structured hexahedral mesh is generated for the test chamber and fins. Cooper hexahedral and wedge mesh is generated for the serpentine bends and channels, while unstructured tetrahedral, hybrid and wedge grids have been created for the rest of the model. These are illustrated in Figure 5 to Figure 8.

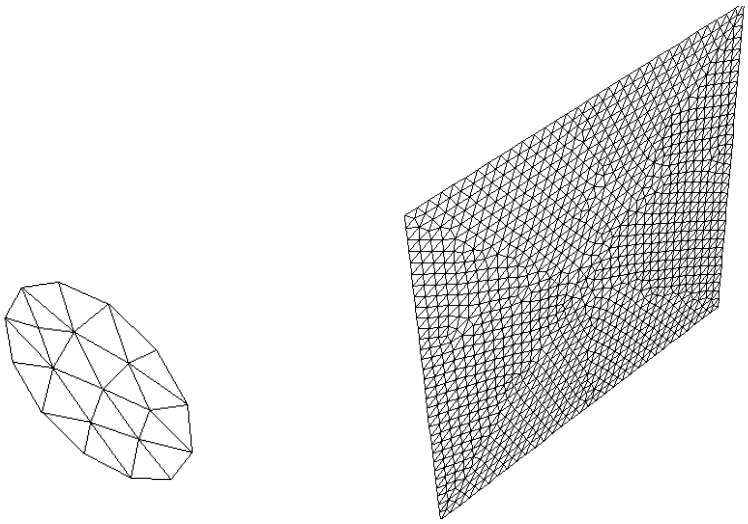

Figure 5. Zoomed channel inlet/outlet mesh (left) and Air inlet/outlet mesh (right).

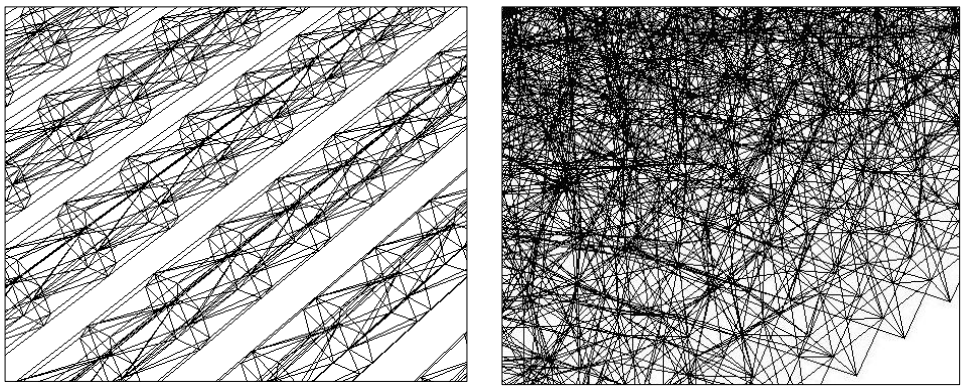

Figure 6. Zoomed channel mesh (left) and zoomed air mesh (right).

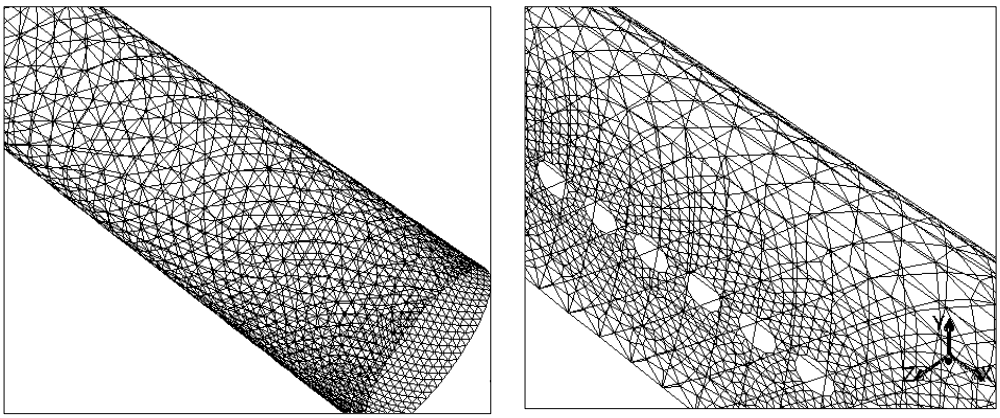

Figure 7. Zoomed inlet and outlet tube mesh (left) and manifold mesh (right).

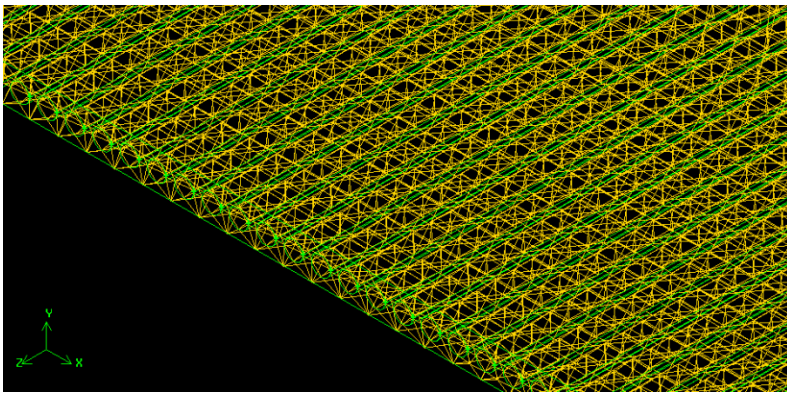

Figure 8. Solid slab mesh (zoomed).

2.4. Assumptions

The computational fluid dynamics (CFD) uses a numerical approach for solving the governing equations. Following assumptions have been made for the given flow geometry and boundary conditions in the current study.

- fluids are single phase incompressible Newtonian fluids.
- thermophysical properties of liquids are the functions of temperature but independent of pressure.
- thermophysical properties of air and solid (aluminium) are constant.
- heat transfer takes place between liquid and air only.
- walls of serpentine, manifolds, and headers are adiabatic.
- there is no diffusion or radiation heat transfer in the system.
- there is no heat loss or gain to or from the surroundings of the test chamber.
- the standard k-ε turbulent model with enhanced wall treatment is used.

2.5. Governing Equations

The Navier-Stokes equations, which properly represent the fluid motion of an incompressible fluid have been considered as the basis of CFD [37]. These equations symbolize mathematical models of the conservation laws of physics including, mass conservation, momentum conservation and energy conservation. In current study, based on some key assumptions, the Reynolds-averaged Navier-Stokes (RANS) equations have been solved by using ANSYS FLUENT 15.0, a finite volume method (FVM) based commercial CFD software. Based on the assumptions and the physics of the problem, the simplified general form of the transport equations are illustrated below.

Continuity or mass conservation: $$\frac{\partial}{\partial x_i}(\rho u_i) = 0 \quad (1)$$

Momentum conservation: $$\frac{\partial}{\partial j}\left(\rho u_i u_j\right) = \frac{\partial}{\partial x_j}\left(\mu \frac{\partial u_j}{\partial x_i}\right) - \frac{\partial P}{\partial x_i} + \frac{\partial}{\partial x_j}\left(-\rho \overline{u_i' u_j'}\right) \quad (2)$$

Energy conservation: $$\frac{\partial}{\partial x_i}(\rho u_i T) = \frac{\partial}{\partial x_j}\left(k_{eff}\frac{\partial T}{\partial x_j} + u_i\left(\tau_{ij}\right)_{eff}\right) \quad (3)$$

where, the effective thermal conductivity, $k_{eff} = k + \frac{C_p \mu_t}{Pr_t}$, the deviatoric stress tensor, $(\tau_{ij})_{eff} = \mu_{eff}\left(\frac{\partial u_j}{\partial x_i} + \frac{\partial u_i}{\partial x_j}\right) - \frac{2}{3}\mu_{eff}\left(\frac{\partial u_k}{\partial x_k}\delta_{ij}\right)$, and Pr_t is the turbulent Prandtl number.

Turbulence kinetic energy, k: $$\frac{\partial}{\partial x_i}(\rho k u_i) = \frac{\partial}{\partial x_j}\left[(\mu + \frac{\mu_t}{\sigma_k})\frac{\partial k}{\partial x_j}\right] + G_k - \rho\epsilon \quad (4)$$

where, the turbulent viscosity, $\mu_t = \rho C_\mu \frac{k^2}{\varepsilon}$ and the term, $G_k = -\rho\overline{u_i' u_j'} \frac{\partial u_i}{\partial x_i}$

Turbulence energy dissipation, ε:

$$\frac{\partial}{\partial x_i}(\rho \varepsilon u_i) = \frac{\partial}{\partial x_j}\left[(\mu + \frac{\mu_t}{\sigma_\varepsilon})\frac{\partial \varepsilon}{\partial x_j}\right] + C_{1\varepsilon}\frac{\varepsilon}{k}G_k - C_{2\varepsilon}\rho\frac{\varepsilon^2}{k} \quad (5)$$

where, $C_{1\varepsilon}, C_{2\varepsilon}$, $C_{3\varepsilon}$, and C_μ are constants, and σ_ε is turbulent Prandtl number for ε.

$$\mu_t = \rho C_\mu \frac{k^2}{\varepsilon} \quad (6)$$

2.6. Grid independency Study

It is essential to note that the mesh fineness plays a vital role in the computational fluid dynamics (CFD) simulations. In the CFD, the simulation time, cost and accuracy greatly depend on proper mesh generation in the computational domain. In order to ensure the accuracy, consistency and reliability of the numerical results, and to retain the computational cost low, the grid indecency test has been performed in the current study. Several grid systems have been used to check grid independency by solving the Navier-Stokes governing equations. These are presented in Figure 9.

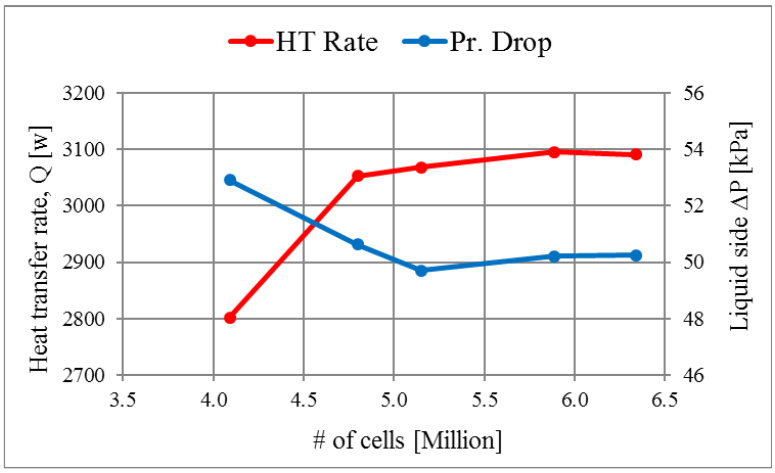

Figure 9. Grid independency study of 2-pass crossflow MICHX.

The relative deviations in the heat transfer rates ($\dot{Q}$) and the pressure drops (ΔP) in two consecutive grid systems (GS) of 2-pass MICHX are evaluated. For $\dot{Q}$, the computed relative deviations between GS1 and GS2, GS2 and GS3, GS3 and GS4, and GS4 and GS5 are 8.95%, 0.52%, 0.88%, and 0.14%, respectively. In case of ΔP, the corresponding variations are found to be 4.32%, 1.81%, 0.99%, and 0.10%. The grid systems have been chosen for the numerical simulations when the maximum variations in both the $\dot{Q}$ and the ΔP in two successive GS are observed about 1%. The number of cells of the selected GS used in CFD simulations of the 2-pass FTHX, MICHX, sequential FTHX, and simultaneous MICHX are 4.36M, 5.89M, 12.49M, and 8.45M, respectively.

2.7. Computational and Physical Setup

The computational and physical parameters, such as model, material properties, boundary conditions, solver, etc. play the major role in the simulation process, the convergence and the accuracy of the solution. In the current study, a three-dimensional, double precision, pressure-based, absolute velocity formulation and implicit scheme has been carried out to solve the flow field and heat transfer problem. Details of the structures of physical and computational fundamental parameters are described in this section.

2.7.1. Model selection

A turbulence model is used to capture the turbulence parameters particularly in thermal and flow fields developed around the air-to-liquid crossflow heat exchanger core. This model is chosen due to the high Reynolds number of the fluids at the inlet and the outlet boundaries as well as three-dimensional unsteady random fluid motion at headers, manifolds, and heat exchanger core. The computational domain includes two continuums, namely liquid and air. The liquid Reynolds number in the heat exchanger core is in the current study is maintained within the range of laminar regime ($350 \leq Re_{ch} \leq 2274$); however the air Reynolds number is in the turbulence flow regime ($3.4 \times 10^4 \leq Re_a \leq 2.1 \times 10^5$). In order to capture the turbulence parameters, a turbulence model is used.

Preliminary simulations have been conducted using Standard k-ε with Std Wall Function (SWF), Standard k-ε with Enhanced Wall Treatment (EWT), Realizable k-ε with EWT, and Shear Stress Transport (SST) k-ω turbulence models. Numerical predictions have been compared to the experimentally measured data. The Standard k-ε with EWT shows better results than the others. As a result, Standard k-ε turbulence model is used in the current study.

The turbulence intensity, I is defined as

$$I = \frac{u'}{u_{ave}} = 0.16 {Re_{d_h}}^{-1/8} \tag{7}$$

where, Re_{d_h}, u' , and u_{ave} are the Reynolds number of fluid based on hydraulic diameter (d_h), the ratio of the root-mean-square of the velocity fluctuations, and the mean velocity of fluid flow.

Viscous heating is enabled to capture the effects of viscous heating on the thermal performance of the heat exchanger.

2.7.2. Properties of materials

All working fluids have been assumed as incompressible within the operating temperature and flow regime. The temperature dependent thermophysical properties of water have been used from the National Institute of Standards and Technology, USA [38].

2.7.3. Boundary conditions

The below boundary conditions have been precisely followed in the current study:

- Inlet liquid: Temperature and mass flow rates are specified.
- Inlet air: Temperature and velocity are specified.
- Outlet liquid: Pressure outlet boundary condition is specified.
- Outlet air: Pressure outlet boundary condition is specified.
- Headers, manifolds and serpentines: Zero heat flux is specified.
- Walls: No slip, stationary, and Type 1 thermal boundary conditions are specified.

2.7.4. Residuals

When successive iteration is stopped, the sum of the normalized absolute residuals in each control volume for the flow and the energy variables have been reduced to 1e-04 and 1e-09, respectively. The intention is to maximize the accuracy of simulation results.

3. Theoretical Background and Data Processing

3.1. Field Variables

ANSYS Fluent Theory Guide [39] has been followed to compute the field variables as

Surface area, A: $$\int dA = \sum_{i=1}^{n} |A_i| \quad (8)$$

Integral of individual field variable, Φ: $$\int \Phi dA = \sum_{i=1}^{n} \Phi_i |A_i| \quad (9)$$

Area-weighted surface temperature: $$\frac{1}{A}\int \Phi dA = \frac{1}{A}\sum_{i=1}^{n} \Phi_i |A_i| \quad (10)$$

Mass-weighted thermophysical properties of working fluids:

$$\left(\int \Phi\rho|\vec{v}\cdot d\vec{A}|\right)/\left(\int \rho|\vec{v}\cdot d\vec{A}|\right) = \left(\sum_{i=1}^{n} \Phi_i\rho_i|\vec{v}_i\cdot\vec{A}_i|\right)\Big/\left(\sum_{i=1}^{n} \rho_i|\vec{v}_i\cdot\vec{A}_i|\right) \quad (11)$$

where, Φ is the field variable (property) of the working fluid, A is the facet (surface) area associated with a cell in the domain, and v is the velocity vector of the working fluid.

3.2. Nusselt number

In heat transfer at a surface boundary within a fluid, Nusselt number is the dimensionless form of convective heat transfer coefficient (h). It signifies the intensification of heat transfer by means of the convection over conduction normal to the boundary. It is defined as

$$Nu = \frac{\text{convective heat transfer}}{\text{conductive heat transfer}} = \frac{h}{k/d} = \frac{hd}{k} \quad (12)$$

Nusselt number is generally expressed as [33]

$$Nu = aRe^{m}Pr^{n} \quad (13)$$

Reynolds number (Re) is the ratio of the inertial forces to viscous forces and determines the flow regime. Prandtl number (Pr) is the ratio of momentum diffusivity (kinematic viscosity) to thermal diffusivity and signifies the thermal and hydrodynamic boundary layer thickness.

3.3. Heat Transfer Evaluation Parameters

Heat transfer rate ($\dot{Q}$): $$\dot{Q} = \dot{m}C_p\Delta T \quad (14)$$

Heat transfer coefficient (h): $$h = \dot{Q}/\left(A_s(T_m - T_s)\right) \quad (15)$$

where A_s is the heat transfer surface area, c_p is the fluid specific heat, $\dot{m}$ is the mass flow rate, ΔT is the temperature difference between fluid enter to and exit from the heat exchanger, T_m is the fluid mean temperature, and T_s is the channel inner surface temperature.

4. Model Verification and Validation

In the current study, initially 2-pass air-to-liquid crossflow FTHX and MICHX are used to investigate basic thermal and fluid flow characteristics. Subsequently, these heat exchangers are used for simulations of sequential and simultaneous modules. With the purpose of quantifying the level of confidence in the CFD results, an organized process and rules have been followed. In that circumstance, verification and validation according to AIAA (1998) [40] and Oberkampf et al. [41] have now been commonly accepted [42]. In order to ensure that the numerical results of the computational model are accurate and consistent, two categories of error analyses namely, verification and validation have been conducted.

4.1. Model Verification

With the aim of minimizing the roundoff error, CFD results have been obtained using a double precision machine with 16-significant digits. A grid independency study has been carried out to ensure that the grid is fine enough to capture the heat transfer and flow fields. Other verifications have been performed by analyzing the errors in the mass flow rate and the heat transfer rate for each simulation. Figure 10 represents the errors in the mass balance (MB) and the heat balance (HB) in numerical results in FTHX and MICHX.

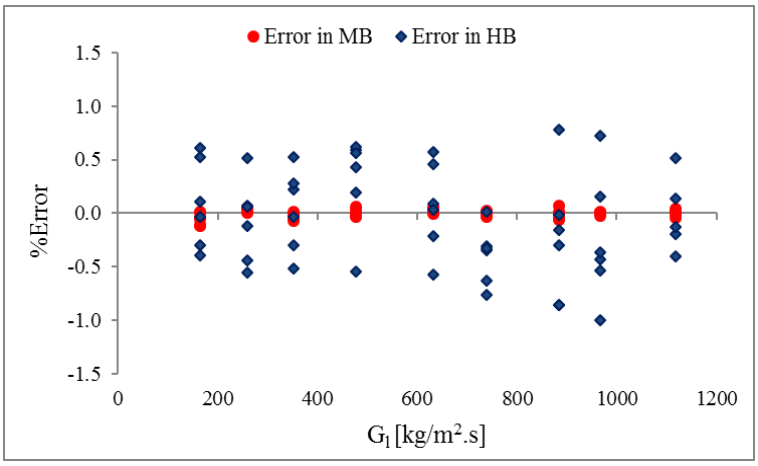

Figure 10. Numerical errors in mass balance (MB) and heat balance (HB).

The errors in mass balance (MB) and heat balance (HB) have been found to be $\pm 0.2\%$ and $\pm 1.1\%$, respectively.

Numerical results have also been evaluated using different computing approaches. Consistent and reliable predictions have been observed in each approach. These are shown in Table 2 and Table 3.

Table 2. Numerical results of 2-pass conventional FTHX at different approaches.

Computation approach	**Results**	
$\dot{Q}_{o/a\_simulation}$	2194.65w	
$Q_{o/a\_calculated} = \dot{m}c_p\Delta T$	2195.37w	
$\dot{Q}_{total} = \sum_{i=1}^{61}(q_{i(top)} + q_{i(bottom)})$	Top = 1224.95w	Bottom = 985.82w
	Total = 2210.77w	
$\bar{h}(x) = \sum_{i=1}^{122} h_i(x) \big/ 122$	$\bar{h}(x)\_top = 5829.52 w/m^2K$ $\bar{h}(x)\_bottom = 5501.71 w/m^2K$ $\bar{h}(x) = 5665.38 w/m^2K$	
$\bar{h}(HX) = Q/A_s(T_b - T_s)$	$\bar{h}(HX) = 5683.971 w/m^2K$	

Table 3. Numerical results of 2-pass MICHX at different approaches.

Computation approach	**Results**	
$\dot{Q}_{o/a\_simulation}$	2443.95w	
$\dot{Q}_{o/a\_calculated} = \dot{m}c_p\Delta T$	2450.05w	
$\dot{Q}_{total} = \sum_{i=1}^{61}\sum_{j=1}^{68}(\dot{q}_{ij(top)} + \dot{q}_{ij(bottom)})$	Top = 1362.09w	Bottom = 1083.51w
	Total = 2445.60w	
$\bar{h}(x) = \sum_{i=1}^{122} h_i(x) \big/ 122$	$\bar{h}_{ch34\_top} = 10109.92 w/m^2K$ $\bar{h}_{ch34_{bottom}} = 9503.55 \frac{w}{m^2K}$ $\bar{h}_{ch34} = 9806.74 w/m^2K$	
$\bar{h}(HX) = \left(\sum_{n=1}^{68} \bar{h}\right) \big/ 68$	$9957.27 w/m^2K$	
$\bar{h}(HX) = \frac{\dot{Q}}{A_s(T_b - T_s)}$	$10063.35 w/m^2K$	

It is obvious from the tables that the heat transfer rates ($\dot{Q}$) and the heat transfer coefficients (h) are almost identical at different evaluation methods. The deviations in $\dot{Q}$ and h at different approaches have been found to be $\pm 0.5\%$ and $\pm 3.9\%$, respectively. These signify the consistency and reliability of the numerical predictions.

4.2. Model Validation with Available Experimental Data

In order to ensure that the model is an accurate representation of the real world from the perspective of the indented uses, a set of simulation results has been compared with experimentally measured data [13]. The operating conditions of both the simulations and experiments are identical. The comparisons, at the laminar flow regime, were mentioned previously in Ismail et al. [17], and these are not repeated here. Good agreement between the numerical predictions and the experimentally measured data was observed. For water, the maximum errors in liquid outlet temperature, air outlet temperature, serpentine temperature, and liquid side pressure drop have been found 0.98%, 1.65%, 1.71% and 13.02%, respectively. The corresponding maximum errors in the parameters have been found 4.79%, 3.02%, 3.88% and 13.25% in case of ethylene glycol. While the mean average errors have been observed between 0.71% to 9.98% for water and 1.61% to 10.21% for ethylene glycol. The verification and validation of numerical results confirm that one can certainly depend on the accuracy and consistency of the CFD models of the current study.

5. Results and Discussions

In this section, the simulation results for sequential and simultaneous modules of conventional FTHX and MICHX are presented. Both the sequential and the simultaneous modules of FTHX and MICHX are identical in slab thickness, frontal area and volume. The same boundary conditions have also been applied for both the heat exchanger modules. Water with two distinct temperatures of 65℃ and 95℃ is cooled by crossflow cold air temperature of 25℃ and velocity of $6\mathrm{m/s}$. Water mass flow rates have been varied within the Reynolds number range of $350 \leq \mathrm{Re} \leq 2250$. The heat exchangers associated with the water inlet temperatures of 65℃ and 90℃ are denoted as MT-HX and HT-HX, respectively. The simulations have been conducted for different Reynolds numbers at laminar flow regime. With the purpose of improving the thermal performance, each module of both the FTHX and the MICHX in various combinations have been simulated and evaluated. For sequential module, the HT-HX is employed in the forward-facing with regard to the incoming cold air, while the MT-HX is placed in the rear of the HT-HX. For simultaneous module, the HT-HX is positioned on the top of the MT-HX. Simulations for simultaneous arrangement have also been carried out using the reverse placement of HT-HX and MT-HX. The particular boundary conditions of the models have been chosen in consideration of the operating conditions of an automotive condenser and radiator when the vehicle runs in the city during the fall.

5.1. Sequential FTHX vs Simultaneous FTHX

Figures 12(a) to 12(c) illustrate the heat transfer rate of simultaneous and sequential modules of FTHX. For sequential module, the MT-HX is placed in front of the HT-HX regarding the ram cold air. For simultaneous module, the HT-HX is positioned on the top of the MT-HX. The figures display that the heat transfer rate increases with increase of Reynolds number for all the cases within the laminar flow regime, as expected. Significant improvement in thermal performance of the HT-HX is observed in simultaneous module than the conventional sequential orientation. Figure 11(a) shows about $10.6\%-17.3\%$ enhanced heat transfer rate in the HT-HX of the simultaneous module. This is because the heat exchanger faces the incoming ambient air in this module, while it receives the outlet warmer air of the MT-HX in sequential module.

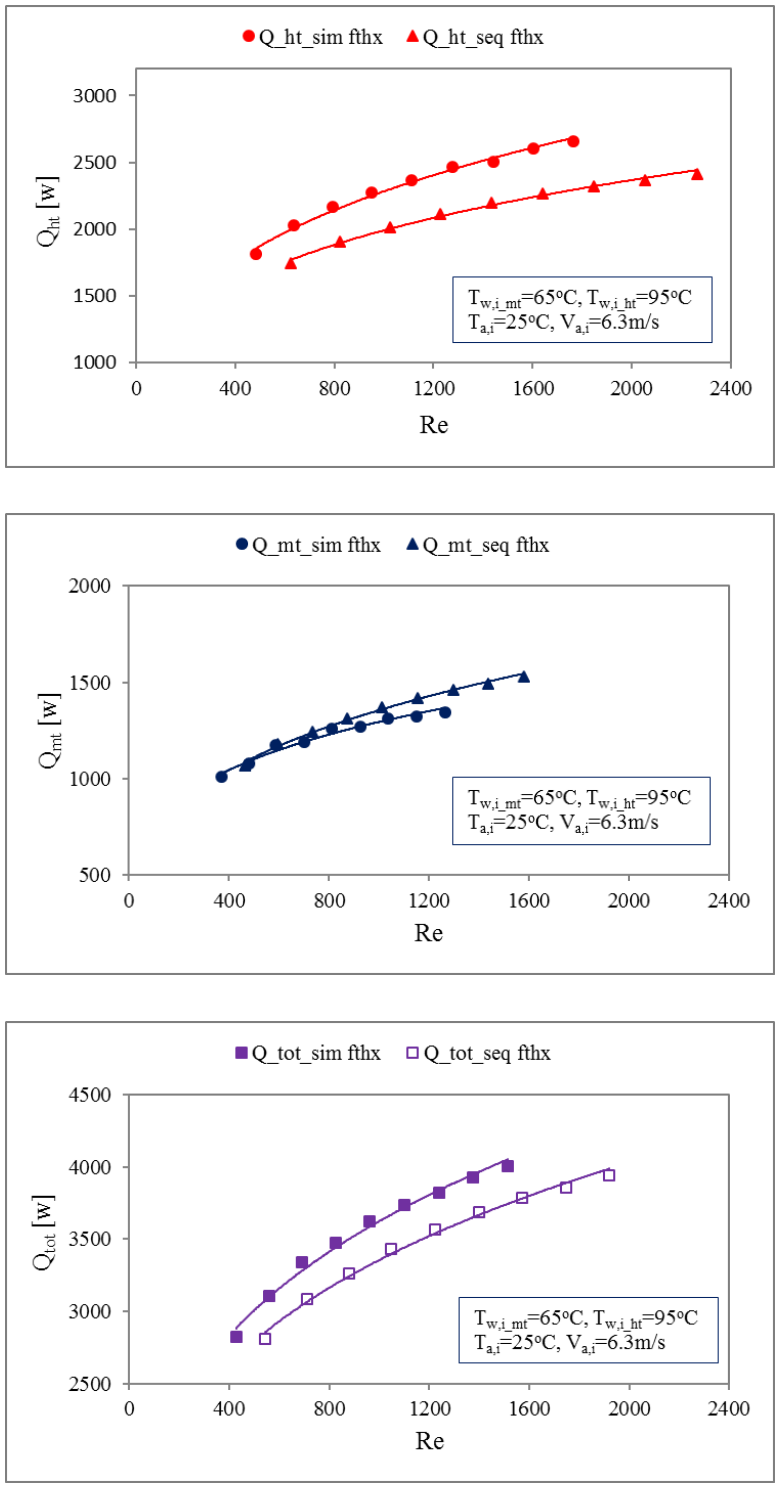

Figure 11. Heat transfer rate of FTHX modules: (a) HT-HX, (b) MT-HX and (c) overall.

The MT-HX displays insignificant improvement or somewhat reduced thermal performance in simultaneous than sequential arrangement, as shown in Figure 11(b). This is because, for both the simultaneous and the sequential arrangement, MT-HX faces identical air of ambient condition, such as quality, velocity, and temperature. However, the MT-HX receives heat from the neighboring HT-HX by means of thermal interaction. At given Re, the overall heat transfer rate of simultaneous FTHX is greater than that of sequential FTHX, as shown in Figure 11(c). Numerical predictions show about 7.5% to 8.1% elevated heat transfer rate for $350 \leq Re \leq 2250$.

5.2. Sequential FTHX vs Simultaneous MICHX

Figures 12(a) to 12(c) illustrate the heat transfer rates of sequential FTHX and simultaneous MICHX modules. Both modules possess similar height, length, width, frontal area, volume and operating conditions. Figures 12(a) and 12(b) represent the numerical predictions of the heat transfer rates through HT-HX and MT-HX, respectively. The overall heat transfer rates of both the modules are presented in Figure 12(c).

(a)

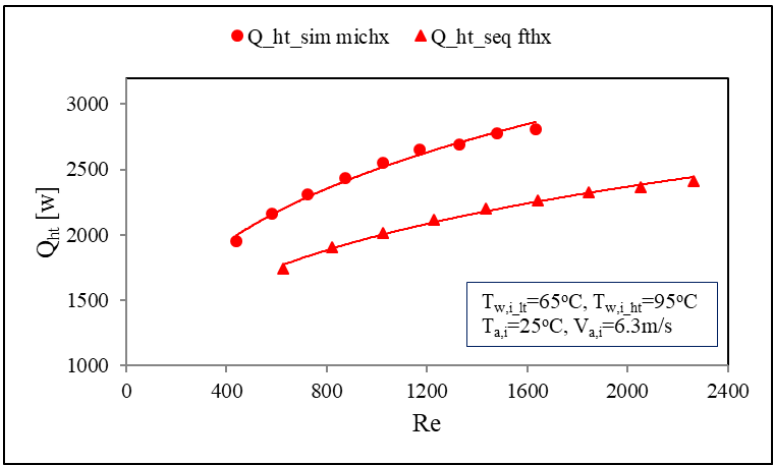

(b)

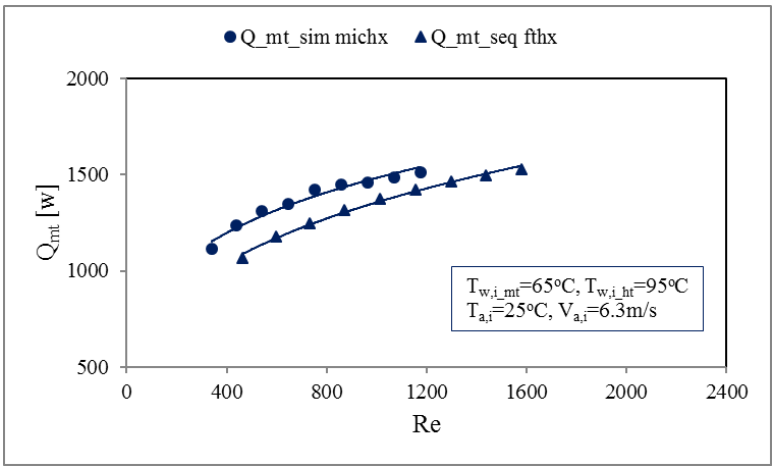

(c)

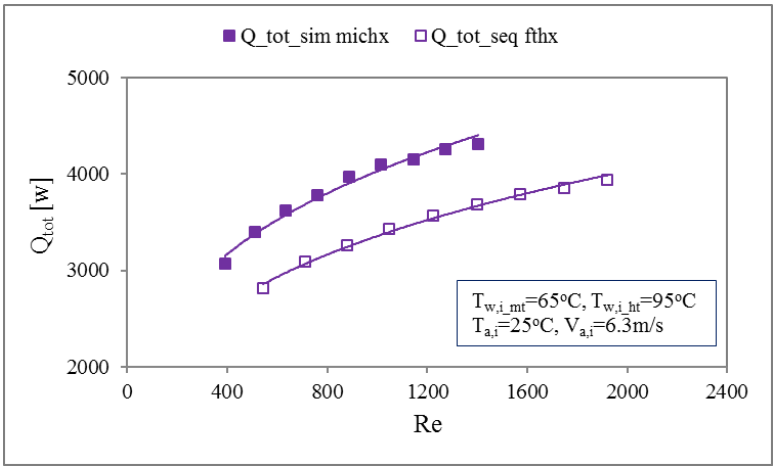

Figure 12. Heat transfer rate of simultaneous MICHX and sequential FTHX: (a) HT-HX, (b) MT-HX and (c) overall.

Figure 12(a) displays higher transfer rate in HT-HX of simultaneous MICHX than that of sequential FTHX within the laminar flow regime. The simultaneous module predicts nearly 22.4% to 27.7% higher heat transfer rate over the sequential module. This is because, in simultaneous module, HT-HX faces the incoming air with ambient conditions; whereas, in sequential module, it receives the outlet warmer air of the MT-HX.

In case of MT-HX, as shown in Figure 12(b), heat transfer rate increases approximately 11.34% in the simultaneous module at low Reynolds, particularly at Re ≈ 400. As Reynolds number increases, the heat transfer rate in the simultaneous module gradually becomes identical to, or somewhat lower than that of the sequential module. This is because, for both the simultaneous and the sequential arrangements, MT-HX faces ambient air with identical quality, velocity, and temperature. However, in simultaneous orientation, the MT-HX receives heat from the neighboring HT-HX by means of thermal interaction. At a particular Re, the overall thermal performance of simultaneous MICHX is superior to that of conventional sequential FTHX. The overall heat transfer rate in simultaneous MICHX is observed to be about 19.8%~20.4% higher compared to that of the sequential FTHX as shown in Figure 12(c).

Figures 13(a) and 13(b) characterize the numerical predictions of h for HT-HX and MT-HX, respectively. The enhancement of h due to employment of simultaneous MICHX for both the HT-HX and the MT-HX is quantified. Within the laminar flow regime, for the HT-HX, the h of simultaneous MICHX module is predicted a 45.9% to 85.4% higher than that of the sequential FTHX module. For the MT-HX, the h of simultaneous MICHX module is found to be about 77%−114.4% higher than that of the sequential FTHX module.

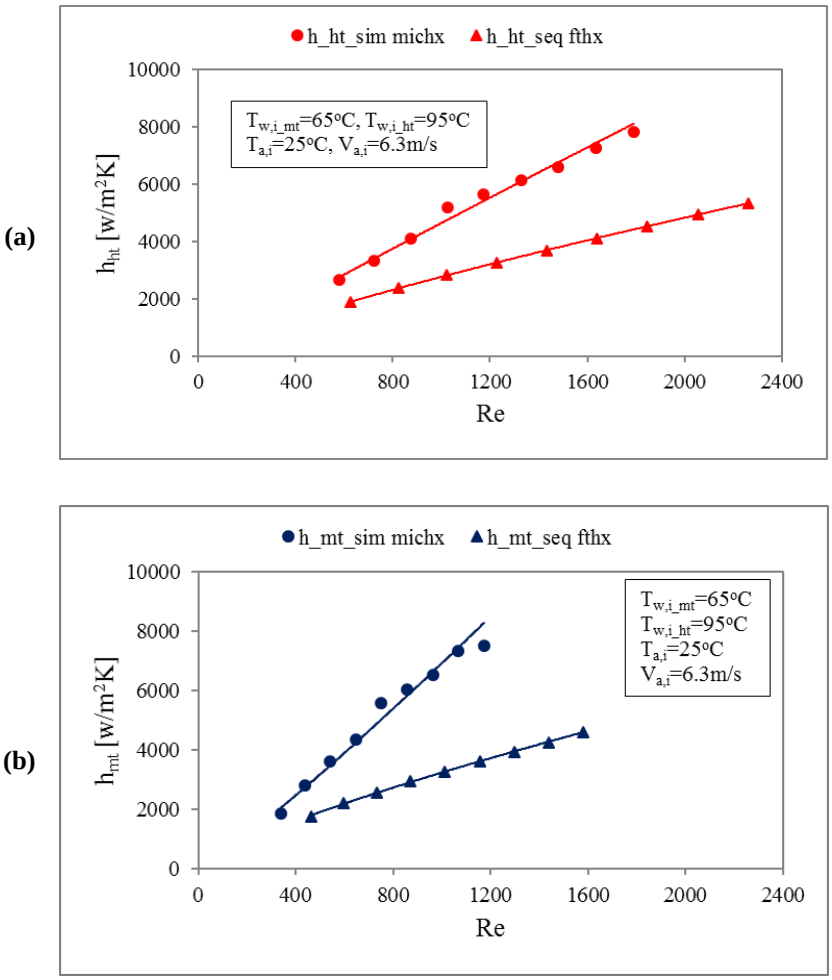

Figure 13. Heat transfer coefficient: (a) HT-HX, (b) MT-HX.

New Nusselt number correlations for both the HT and the LT of each module have been obtained in the form of $Nu = ARe^{m}Pr^{n}$. The correlations are in. The developed correlations are illustrated in Figures 14(a) and 14(b).

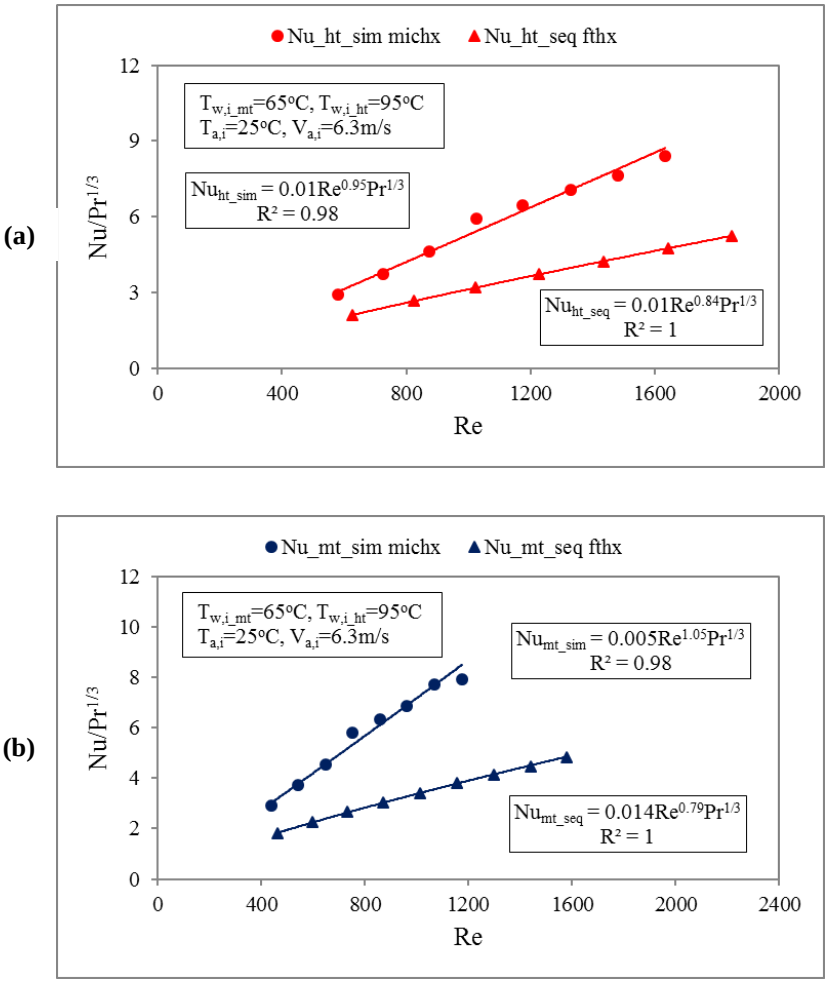

Figure 14. Nusselt number correlations: (a) MT-HXs and (b) HT-HXs.

5.3. Simultaneous MICHX vs Simultaneous FTHX

The thermal performance of simultaneous modules of the MICHX and the FTHX have been evaluated with intention of making the most effective use of the modules and presented in Figures 15(a) to 15(c).

It is seen in Figures 15(a) and 15(b) that the heat transfer rates in both the HT-HX and the MT-HX are higher in simultaneous MICHX than that of the FTHX. Consequently, the overall heat transfer rate is also greater in the MICHX module, as shown in Figure 15(c).

The $Q_{enh.}$ of simultaneous modules of both the MICHX and the FTHX have been assessed with reference to an identical sequential FTHX module as a benchmark. They provide greater heat transfer rates than the sequential module. Between the two simultaneous modules, MICHX provides belter thermal performance than FTHX. The numerical results predict approximately 10.6% and 11% higher heat transfer rate for the HT-HX and MT-HX, respectively at the simultaneous MICHX module than that of the FTHX module.

5.4. Effect of Placement of HT-HX and MT-HX in Simultaneous MICHX Module

The effect of the placement sequence of the HT-HX and MT-HX in simultaneous MICHX

module is also predicted for building the best operational use of the resource. Two options are available for the positioning of the heat exchangers in the simultaneous module. Option-1: HT-HX on the top and MT-HX in the bottom and Option-2: MT-HX on the top and HT-HX in the bottom. The heat transfer rates for the both options are illustrated in Figures 16.

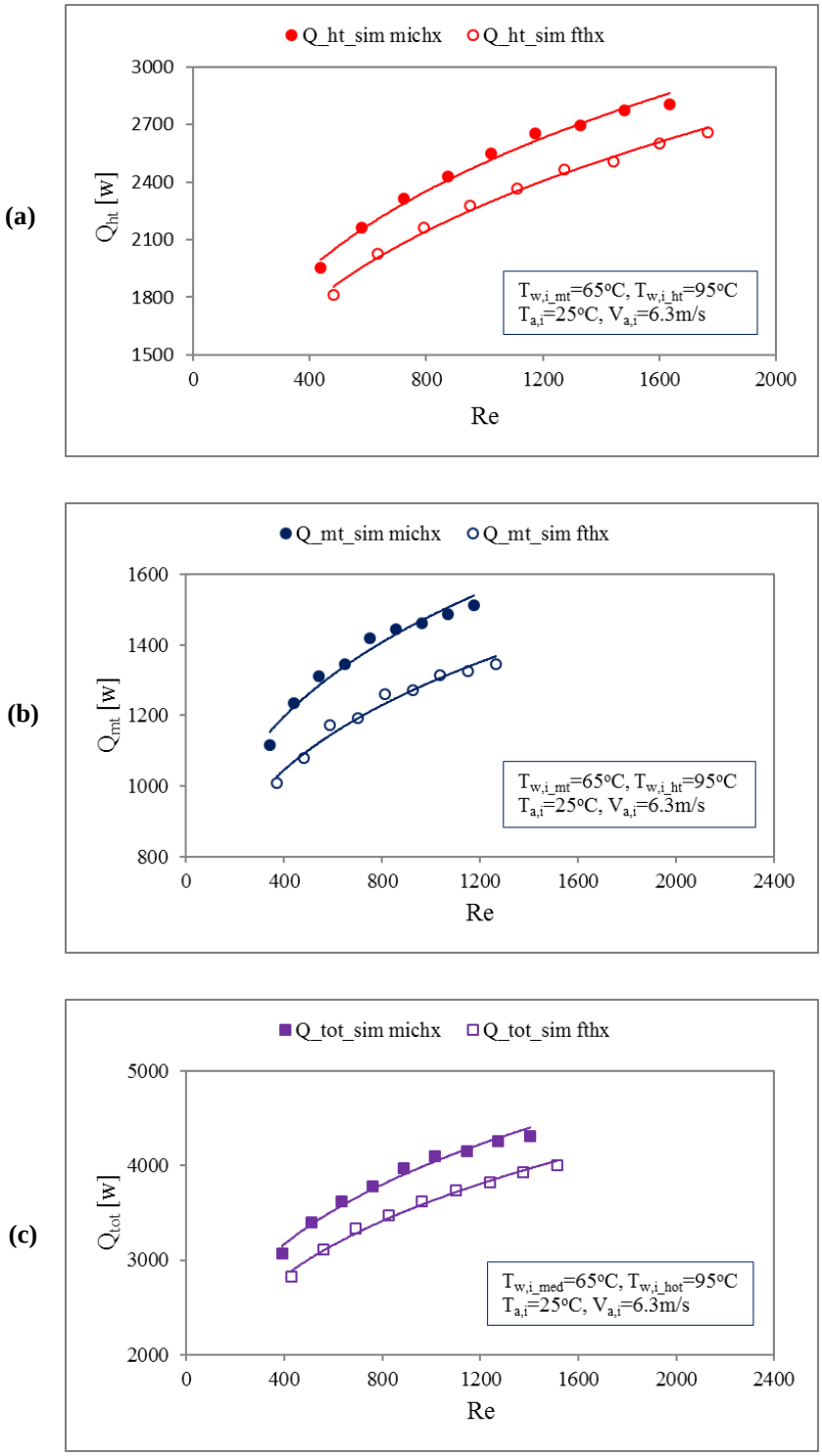

Figure 15. Heat transfer rate: (a) HT-HXs, (b) MT-HXs and (c) Overall.

In this figure, the solid and dashed lines represent the heat transfer rate for Option-1 and Option-2, respectively. It is obvious from the figure that the position of the heat exchangers

significantly effects on the thermal performance of individual heat exchanger. The figure shows that both the HT and MT heat exchangers provide higher heat transfer rate when they have been placed in the bottom. This is due to the thermal boundary conditions and thermal interactions between HT-HX and MT-HX. The inlet slab of the top heat exchanger and the outlet slab the bottom heat exchanger are with the contact of adiabatic wall surfaces. On the other hand, the outlet slab of the top heat exchanger makes contact with the inlet slab of the bottom heat exchanger. Consequently, the thermal interaction takes place between two the heat exchangers. This phenomenon significantly effects the heat transfer rate. The intensity of the thermal interaction depends on the position of HT-HX and MT-HX. In fact, it is not feasible to place both the heat exchangers at the same position in a module. Depending on the thermal system requirements, decision needs to be taken for positioning the order of HT-HX and MT-HX. The overall heat transfer rates for both Option-1 and Option-2 are identical. This is because of the fact that both the heat exchangers work as a single unit. They have been cooled by crossflow air within a single domain of adiabatic wall.

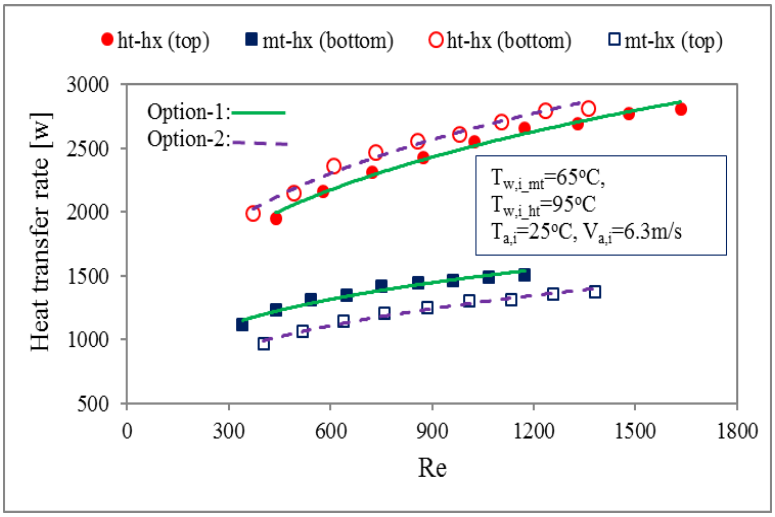

Figure 16. Comparison of heat transfer rate of HT-HX and MT-HX between two discrete placement options.

6. Conclusions

The current research has been intended to achieve detailed numerical investigative analyses with sequential and simultaneous heat exchanger modules to characterize and improve heat transfer performance based on arrangement. The simultaneous heat exchanger module outperforms the conventional sequential module as a benchmark. For a given Reynolds number within the laminar flow regime, simultaneous MICHX module provides even more heat transfer over the FTHX module. Simultaneous MICHX module offers nearly 20%−25% elevated heat transfer rate than that of the sequential FTHX. Whereas, the FTHX if oriented to simultaneous arrangement, offers nearly 10%−12% increased heat transfer rate compared to its previous sequential orientation. The intensification of heat transfer coefficient in simultaneous MICHX have been predicted to be about 46% to 85% for HT-HX and 77% to 114% for MT-HX. In simultaneous module, the position of heat exchangers (HXs) significantly affects the thermal performance of the HXs. Both the HT-HX and the MT-HX provide higher heat transfer rate if these have been positioned in the bottom. However, it is not feasible to place both HXs at the same location in a module. The placement of heat exchanger, therefore, depends on the requirements of the thermal systems.

The proposed simultaneous MICHX module, where both HXs will face similar incoming air with the equivalent ambient conditions can significantly improve the heat transfer performance.

It can reduce the operational energy requirements in applications, especially in automotive HVAC and cooling systems. It can also improve life cycle climate performance (LCCP) and mitigate the emission standards set by the EPA and the CARB.

Acknowledgements

The authors are thankful to the Natural Sciences and Engineering Research Council of Canada (NSERC) for providing discovery grant (NSERC-DG) for conducting the research work. The authors also gratefully acknowledge the department of Mechanical, Automotive, and Materials Engineering at University of Windsor for providing the Post-Doc opportunity for current and ongoing research.

References

[1] Enerdata 2018, "Global energy statistical yearbook 2018."

[2] EPA, "Inventory of U.S. Greenhouse Gas Emissions and Sinks: 1990-2015," 2017.

[3] BPstats, BP Statistical Review of World Energy, 67th ed. UK: BP plc, 2018.

[4] Environment and Climate Change Canada, "National inventory report 1990-2015: Greenhouse gas sources and sinks in Canada," United Nations Framework Convention on Climate Change, 2017.

[5] OICA, "International Organization of Motor Vehicle Manufacturers, Production Statistics," 2017.

[6] Y. Zhai, G. Xia, Z. Li, and H. Wang, "Experimental investigation and empirical correlations of single and laminar convective heat transfer in microchannel heat sinks," Exp. Therm. Fluid Sci., vol 83, pp. 207-214, 2017.

[7] M. E. Steinke and S. G. Kandlikar, "Single-phase heat transfer enhancement techniques in microchannel and minichannel flows," in The 2nd International Conference on Microchannels and Minichannels, pp. 1-8, 2004.

[8] M. S. Saadi, M. Ismail, S. Fotowat, M. A. Quaiyum, and A. Fartaj, "Study of motor oil cooling at low Reynolds number in multi-port narrow channels," SAE Int. J. Engines, vol 6, no. 2, pp. 1287-1298, 2013.

[9] M. A. Quaiyum, A. Fartaj, and S. Askar, "An experimental characterization of automatic transmission fluid flowing through air cooled microchannel heat exchanger," SAE Int. J. Mater. Manf., vol 5, no. 2, pp. 503-516, 2012.

[10] M. A. Quaiyum, M. Ismail, and A. Fartaj, "Study of automatic transmission fluid in a serpentine minichannel heat exchanger: An experimental approach," Exp. Heat Transf., vol. 28, no. 3, pp. 244-266, 2015.

[11] J. Liu, S. Hussain, W. Wang, L. Wang, G. Xie, and B. Sundén, "Heat transfer enhancement and turbulent flow in a rectangular channel using perforated ribs with inclined holes," J. Heat Transfer, vol 141, pp. 1-15, 2019.

[12] Z. Li, W. Q. Tao, and Y. L. He, "A numerical study of laminar convective heat transfer in microchannel with non-circular cross-section," Int. J. Therm. Sci., vol 45, pp. 1140-1148, 2006.

[13] M. G. Khan, "Experimental investigation of heat transfer and pressure drop characteristics of water and glycol-water mixture in multi-port serpentine microchannel slab heat exchangers," Ph.D. dissertation, Dept. Mech. Auto. Mat. Eng., Univ. Windsor, ON, Canada, 2011.

[14] S. G. Kandlikar, "A roadmap for implementing minichannels in refrigeration and air-conditioning systems - Current status and future directions," Heat Transf. Eng., vol 28, no. 12, pp. 973-985, 2007.

[15] A. Jokar, S. J. Eckels, and M. H. Hosni, "Single-phase flow in meso-channel compact heat exchangers for air conditioning applications," Heat Transf. Eng., vol 31, no. 1, pp. 3-16, 2010.

[16] M. Ismail, S. Fotowat, and A. Fartaj, "Effect of channel size on heat transfer and pressure drop in thin slabs minichannel heat exchanger," Int. J. Mech. Eng. Mechatronics, vol 2, no. 1, pp. 32-41, 2014.

[17] M. Ismail, A. Fartaj, and M. Karimi, "Numerical investigation on heat transfer and fluid flow behaviors of viscous fluids in a minichannel heat exchanger," Numer. Heat Transf. Part A Appl., vol 64, no. 1, pp. 1-29, 2013.

[18] Y. Fan and L. Luo, "Recent applications of advances in microchannel heat exchangers and multi-scale design optimization," Heat Transf. Eng., vol 29, pp. 461-474, 2008.

[19] E. S. Dasgupta, F. A. Siddiqui, and A. Fartaj, "Experimental study on air side heat transfer and fluid flow characteristics of microchannel heat exchanger," SAE Int. J. Mater. Manuf, vol 4, no. 1, pp. 1198-1210, 2012.

[20] E. S. Dasgupta, S. Askar, M. Ismail, A. Fartaj, and M. A. Quaiyum, "Air cooling by multiport slabs heat exchanger: An experimental approach," Exp. Therm. Fluid Sci., vol 42, pp. 46-54, 2012.

[21] N. B. Chien, P. Q. Vu, N. M-Ghazali, and O. J-Taek, "Convective heat transfer characteristics of single phase liquid in multiport minichannel tube: Experiment and CFD simulation," Energy Procedia, vol 75, pp. 3180-3185, 2015.

[22] F. A. Siddiqui, E. S. Dasgupta, and A. Fartaj, "Experimental investigation of air side heat transfer and fluid flow performances of multi-port serpentine cross-flow mesochannel heat exchanger," Int. J. Heat Fluid Flow, vol 33, no. 1, pp. 207-219, 2012.

[23] C. A. Balaras, "A review of augmentation techniques for heat transfer surfaces in single-phase heat exchangers," Energy, vol 15, no. 10, pp. 899-906, 1990.

[24] A. E. Bergles, "ExHFT for fourth generation heat transfer technology," Exp. Therm. Fluid Sci., vol 26, pp. 335-344, 2002.

[25] A. E. Bergles, M. K. Jensen, and B. Shome, "The literature on enhancement of convective heat and mass transfer," J. Enhanc. Heat Transf., vol 4, pp. 1-6, 1996.

[26] A. E. Bergles, Enhanced heat transfer: Endless frontier, or mature and routine? Applied Optical Measurements, Springer-Verlag Berlin Heidelberg, 1999.

[27] M. G. Khan and A. Fartaj, "A review on microchannel heat exchangers and potential applications," Int. J. Energy Res., vol 35, pp. 553-582, 2011.

[28] I. Papautsky, T. Ameel, and A. B. Frazier, "A review of laminar single-phase flow in microchannels," in ASME International Mechanical Engineering Congress and Exposition (IMECE2001), pp. 1-9, 2001.

[29] W. Q. Tao, Y. L. He, Q. W. Wang, Z. G. Qu, and F. Q. Song, "A unified analysis on enhancing single phase convective heat transfer with field synergy principle," Int. J. Heat Mass Transf., vol 45, no. 24, pp. 4871-4879, 2002.

[30] S. Kandlikar, "Effect of liquid-vapor phase distribution on the heat transfer mechanisms during flow boiling in minichannels and microchannels," Heat Transf. Eng., vol 27, no. 1, pp. 4-13, 2006.

[31] T. L. Bergman, A. S. Lavine, F. P. Incorpera, and D. P. Dewitt, Fundamentals of heat and mass transfer, 7th ed. John Wiley & Sons, Inc, USA, 2011.

[32] F. M. White, Heat and mass transfer, 1st ed. Reading, Mass. : Addison-Wesley, 1988.

[33] Y. A. Cengel, Heat and Mass Transfer (SI Units): A Practical Approach, 3rd ed. McGraw Hill, 2006.

[34] S. G. Kandlikar and W. J. Grande, "Evolution of microchannel flow passages-thermohydraulic performance and fabrication technology," Heat Transf. Eng., vol 24, no. 1, pp. 3-17, 2003.

[35] M.-H. Kim and C. W. Bullard, "Performance evaluation of a window room air conditioner with

microchannel condensers," J. Energy Resour. Technol., vol 124, no. 1, pp. 47-55, 2002.

[36] J. H. Kim and E. A. Groll, "Performance comparisons of a unitary split system using microchannel and fin-tube outdoor coils, Part I: Cooling tests," Int. Refrig. Air Cond. Conf., no. Paper 557, pp. 219-229, 2002.

[37] J. Peiro and S. Sherwin, Handbook of materials modeling. Volume I: Methods and models, S. Yip. Netherlands: Springer, 2005.

[38] NIST, "Thermophysical properties of fluid systems," National Institute of Standards and Technology. 2017.

[39] ANSYS Inc., ANSYS Fluent Theory Guide, R15 ed. Canonsburg, USA, 2013.

[40] AIAA (1998), "Guide for the verification and validation of computational fluid dynamics simulations," AIAA G-077-1998(2002).

[41] W. L. Oberkampf, T. G. Trucano, and C. Hirsch, "Verification and validation for modeling and simulation in computational science and engineering," in Foundations for Verification and Validation in the 21st Century Workshop, pp. 1-74, 2002.

[42] H. Versteeg and W. Malalasekera, Introduction to computational fluid dynamics-The finite volume method, 2nd ed. Pearson Education Ltd, England, 2007.

Biographical Information

Mohammed Ismail obtained Bachelor of Science (BSc) in Mechanical Engineering in 1993 from Bangladesh University of Engineering and Technology (BUET). He received Master of Applied Science (MASc) in 2012 and Doctor of Philosophy (PhD) in 2019, both in Mechanical Engineering from the University of Windsor, Ontario, Canada under supervision of Dr. Amir Fartaj. His research focused on the HVAC and thermal flow systems. The outcomes of his research resulted in various peer-reviewed journals and conference proceedings. He presented his research findings in several International Conferences in North America. He worked in multiple manufacturing industries for more than twelve years. Currently, he is employed as a Post-Doctoral Fellow in the Department of Mechanical Automotive and Materials Engineering (MAME) at University of Windsor.

Mesbah G. Khan obtained Bachelor of Science (BSc) in Mechanical Engineering in 1986 from Rajshahi University of Engineering and Technology (RUET), Bangladesh. He received Master of Science (MSc) in Renewable Energy in 2000 from University of Oldenburg, Germany. He completed Master of Applied Science (MASc) in 2004 and Doctor of Philosophy (PhD) in 2011, both in Mechanical Engineering from the University of Windsor, Ontario, Canada. His research focus was Thermo-fluids, Heat transfer and Mini-channel thermal systems. He has a number of Journal and Conference publications in Heat transfer, Heat exchangers, HVAC and Thermal energy systems. He worked as Mechanical & Thermal Systems Design Engineer in senior capacities in a number of industries i.e. Energy utility operator, HVAC thermal systems design OEM, A/C compressor and HVAC module manufacturing OEM industries in total more than 22 years. Currently, he is serving as a Senior Mechanical Engineer at Sanden International (USA) Inc. at its Technical Center of America in Michigan, USA.

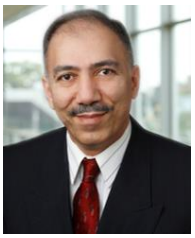

Amir Fartaj has been a heat transfer and thermodynamic educator for more than 18 years in the Department of Mechanical Automotive and Materials Engineering (MAME) at University of Windsor. He has experience as an HVAC and refrigeration consultant and design engineer for air conditioning companies. His main expertise is in the experimental and analytical heat transfer field. He has supervised and graduated more than 20 PhD and MASc students within the past ten years. All researchers are highly trained in theory, modeling and experiments related to their field of study. They also benefited from the opportunity to learn from their applied research to solve real-world problems faced by industry.